Research Article | Vol. 30, No. 22 / 24 Oct 2022 / Optics Express 40425
Optics EXPRESS

Designing multi-mode anti-resonant hollow-core fibers for industrial laser power delivery

WILLIAM SHERE,* ERIC NUMKAM FOKOUA, GREGORY T. JASION, AND FRANCESCO POLETTI

Optoelectronics Research Centre, University of Southampton, Southampton SO17 1BJ, United Kingdom
*w.shere@soton.ac.uk

Abstract: We investigate the design of hollow-core fibers for the delivery of 10s of kilowatt average power from multi-mode laser sources. For such lasers, delivery through solid-core fibers is typically limited by nonlinear optical effects to 10s of meters of distance. Techniques are presented here for the design of multi-mode anti-resonant fibers that can efficiently couple and transmit light from these lasers. By numerical simulation we analyze the performance of two anti-resonant fibers targeting continuous-wave lasers with M^2 up to 13 and find they are capable of delivering MW-level power over several kilometers with low leakage loss, and at bend radii as small as 35 cm. Pulsed lasers are also investigated and numerical simulations indicate that optimized fibers could in principle deliver nanosecond pulses with greater than 100 mJ pulse energy over distances up to 1 km. This would be orders of magnitude higher power and longer distances than in typical machining applications using the best available solid core fibers.

1. Introduction

In recent years, rapid progress in the fabrication of hollow-core anti-resonant fibers (ARF) has proven the theoretical promise of the technology. The past two years have seen reports of nested anti-resonant nodeless fibers (NANFs) with 0.28 dB/km loss at telecommunication wavelengths, only marginally higher than solid-core silica fiber [1], all-time record low-loss transmission in any type of optical fiber at shorter wavelengths eg 0.3 dB/km at 1060 nm [2], and more recently the first double-nested fiber (DNANF) with 0.174 dB/km attenuation at 1550 nm, on par with that of commercial solid-core single-mode fibers [3]. With the performance of these fibers now proven and further loss reduction still possible, the focus of research is turning to applications that can exploit their low non-linearity, latency and dispersion [4], exceptional polarization purity [5], ultralow backscattering [6] and low loss.

High-power fiber delivery is one such application. It typically employs solid-core large-mode-area or large-core multi-mode fibers, primarily limited by the onset of nonlinear processes [7]. The maximum power distance product before stimulated Raman scattering significantly modifies the signal is given by $P \cdot L_{\text{eff}} = 16A_{\text{eff}}/g_r$, where P is the laser power, L_{eff} is the effective interaction length of the fiber, A_{eff} is the effective interaction area and g_r is the Raman gain coefficient (for a large core, multi-mode silica fiber $L_{\text{eff}} \approx L$ when L<100 m, $A_{\text{eff}} \approx \pi(0.8R)^2$ and $g_r = 1 \times^{-13}$ mW^{-1}) [8]. Higher powers delivered over a short distance experience the same nonlinear behaviour as low power delivered over long distances. In solid-core fibres, transmission of 1 kW of power over 100 m has been reported in a highly multi-mode (~750 modes) step-index fibre [9] and 10 kW over 30 m has been demonstrated in a three-mode photonic crystal fibre [10]. Commercially available solutions are typically limited to a few 10s of meters e.g. a commercial multi-mode 10 kW fiber laser has 100 µm delivery fiber up to 30 m long [11]. ARFs by contrast intrinsically possess greatly reduced optical nonlinearity compared to silica fibers since the overlap between the silica and propagating light is less than 1×10^{-4} [4] and the

#473681 https://doi.org/10.1364/OE.473681
Journal © 2022 Received 24 Aug 2022; revised 30 Sep 2022; accepted 3 Oct 2022; published 17 Oct 2022

Optics EXPRESS

nonlinear coefficient of air is almost three orders of magnitude lower than silica [12]. The unique properties of ARFs raise the potential for significant improvements in reach, flexibility and power handling capabilities of their solid-core counterparts.

Practical demonstrations of laser power delivery through hollow-core fibers have greatly progressed over the past two decades [13–16], culminating in the recent remarkable demonstration of 1 kW continuous-wave (CW) power transmitted over 1 km of single-mode NANF [17]. This body of work has so far focused on the transmission of high quality, single-mode laser beams with low M^2. Greater laser power still is available from few-mode and multi-mode lasers [18], and there are a broad range of applications which would benefit from the ability to deliver such lasers across long distances using fibers.

The performance of such few-mode/multi-mode high-power laser sources has also seen great progress in recent years [18]; the markers in the plot shown in Fig. 1 represent a selection of commercially available or research grade lasers of various architectures, both pulsed or cw, emitting near 1030 nm. Higher power lasers in general are effectively few-moded or multi-moded (MM), exhibiting larger M^2 values. To efficiently couple light from these sources into a fiber requires a similarly few-mode or MM fiber. To illustrate this, we show on the same plot the calculated approximate number of mode groups a hollow-core fiber must guide to achieve at least 95% coupling efficiency to a laser source with a given M^2 value (details of the calculation are given in Section 2). It is clear therefore that to meet the needs of applications requiring the flexible delivery of optical power from such lasers over some distance, we must design low loss multi-mode hollow-core fibers.

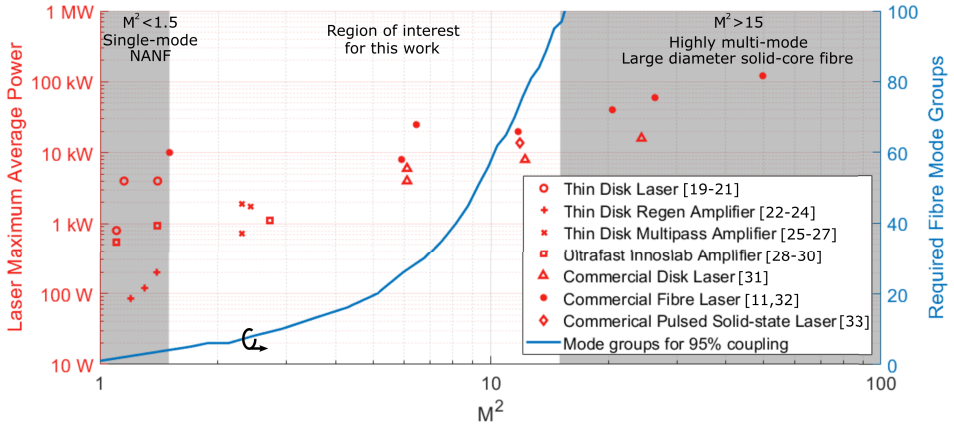

Fig. 1. (red markers, left axis) The maximum average power output of high power laser sources and their reported M^2 values [11,19–33]. (blue line, right axis) The number of mode groups required to be guided in a hollow-core fiber to achieve 95% coupling efficiency for an incident laser beam of a given M^2. The laser described by [32] is characterized only as single-mode and we assume $M^2 = 1.5$.

In the present work, the range of sources we target for ARF delivery (highlighted in Fig. 1), comprises lasers with output powers ranging from 1 to 30 kW with reported M^2 values from 1.5 to 15. For M^2 values below the region of interest, i.e., M^2<1.5, the near diffraction-limited, approximately single-mode lasers emitting up to several kW average power can be delivered, as shown by the results of Mulvad et al. [17], through single-mode NANFs over several kilometers (e.g. Mulvad et al. predict the delivery of 5 kW over more than 2 km with an air-filled core). Above the region of interest, M^2>15 laser sources can emit more than 100 kW average power [11]. These lasers are highly multi-mode (ie. more than 100 mode groups) and fiber delivery is typically through highly multi-mode solid-core fibers with core diameters as large as 800 µm [11].

Optics EXPRESS

It is conceivable that ARFs might one day be designed to guide the several 100s of mode groups required to efficiently couple light from these sources, however, it is not the focus of this work. We focus instead on the intermediate range $1.5<M^2<15$ where MM ARFs can offer significant improvements on the performance of solid-core fibers.

The focus on hollow-core research so far has mostly been on achieving record performance whilst maintaining effectively single mode operation. This is achieved by designing the fiber structure so that orders of magnitude greater leakage loss is imposed on the higher-order modes without affecting the fundamental mode. There are, however, a broad range of applications that could benefit from few- or multi-mode ARFs including short-haul telecomms [34], sensing [35] and, as discussed here, power-delivery. Multi-mode operation can be achieved by altering the design of the fiber cladding to achieve an acceptably low intermodal differential loss. A few recent works have investigated the possibility of guiding more than one mode group [36–38] but have been limited to < 10 mode groups ($M^2<3$) which would still fall short of the requirements for efficient coupling and delivery of high power lasers in our range of interest.

In this work we examine MM ARFs that can deliver power from laser sources with $1.5<M^2<15$. A robust technique is presented for the design of MM ARF capable of guiding the number of modes required to efficiently capture light from sources with given M^2 values in this range. Using numerical simulations, we study the loss-limited distances over which power can be delivered through fibers designed using our proposed method. Our best designs offer in theory less than 0.5 dB loss after 2 km of propagation, even when bent at a 35 cm bend radius. Current CW laser sources in the range of interest are capable of emitting up to 30 kW average power whereas, the fibers we propose can withstand more than 1 MW CW before incurring damage. We also study and optimize the fibers for the delivery of high peak-power pulsed lasers. We find that for picosecond and shorter pulses, delivery through MM ARFs is limited to 10s of meters by the fibers' differential group delay which would broadens the pulses as they propagate. For longer, nanosecond pulses however, MM ARFs seem capable of delivering pulses over > 1 km distance with at least 20x higher energy than the highest energy commercial nanosecond pulsed laser of which we are aware with M^2 in the range of interest [39].

The paper is organized as follows: Section 2. describes the methods we use to characterize laser beams and determine the number of modes required for efficient coupling in hollow-core fibers. Section 3. discusses multi-mode guidance in ARF and describes the techniques we have developed for designing MM NANFs to achieve modality and loss specifications. Section 4. studies, by numerical simulation, two example fibers designed using our techniques and discusses their performance for high power MM laser power delivery. In Section 5. we summarize the work.

2. Coupling of multi-mode laser beams into multi-mode ARFs

The quality of a beam is often characterised by the M^2 factor defined as the ratio of the beam parameter product to that of an ideal, diffraction-limited Gaussian beam [40]. The highest possible beam quality is achieved with $M^2 = 1$ and the power is fully transmitted in the lowest divergence fundamental mode. Greater M^2 values correspond to beams with larger divergence angles caused by a fraction of the total power being transmitted by higher-order and higher divergence modes. Since the transverse profile of these modes differs from that of the near-Gaussian fundamental mode, beams with a larger M^2 will not couple efficiently into single-mode fiber and MM delivery fibers are required for adequate coupling efficiency.

For example, a MM step-index fiber with numerical aperture 0.22 and core diameter 50 µm will guide several 100s of modes and the larger cores typically used for high power delivery can guide many times more. The highly multi-mode nature of these fibers mean they can easily achieve efficient coupling for large M^2 beams. In hollow-core anti-resonant fibers the guidance mechanism results in strong differential properties between modes, with higher order

Optics EXPRESS

modes generally exhibiting higher losses, higher dispersion and higher overlap with the glass. Knowledge of the number of modes required to accommodate a beam with a given M^2 is therefore crucial in designing the fiber.

In high-power delivery through fiber, high input coupling efficiency is necessary both to achieve high throughput and to avoid thermal damage to the input facet of the fiber since the laser energy that is not coupled into the core may be absorbed by the coating near the fiber end face and damage it. In this work we target the design of fibers enabling at least 95% coupling efficiency to a given MM laser source. This is the highest efficiency we are aware of being practically reported in ARF [41]. Such high coupling efficiency should reduce the requirement for active cooling at the fiber coupling and enable further power upscaling. To investigate this target, we consider how the modes of an ARF are excited by an incident field. These modes form a complete, orthogonal set and are normalized such that for any mode labelled k and k':

$$\iint \vec{\mathbf{z}}\cdot(\mathbf{E}_k\times\mathbf{H}^*_{k'} + \mathbf{E}^*_{k'}\times\mathbf{H}_k)dA = \delta_{k,k'} \tag{1}$$

where $\mathbf{E}_k$, $\mathbf{H}_k$ are the electric and magnetic fields of the k^{th} fiber mode and $\delta_{s,u}$ is the Kronecker delta, which evaluates to 1 if $s = u$ and 0 otherwise. Since the modes form a complete set, any incident field, $\mathbf{E}^{(\text{i})}$ and $\mathbf{H}^{(\text{i})}$, can be described as a linear combination of the modes:

$$\mathbf{E}^{(\text{i})} = \sum_k c_k\mathbf{E}_k, \qquad \mathbf{H}^{(\text{i})} = \sum_k c_k\mathbf{H}_k \tag{2}$$

with c_k the amplitude coupling coefficient into mode k given by:

$$c_k = \iint \vec{\mathbf{z}}\cdot(\mathbf{E}^{(\text{i})}\times\mathbf{H}^*_k + \mathbf{E}^*_k\times\mathbf{H}^{(\text{i})})dA \tag{3}$$

If the incident field, $\mathbf{E}^{(\text{i})}$ and $\mathbf{H}^{(\text{i})}$, has been normalised according to Eq. (1) to carry unit power then $|c_k|^2$ describes the power coupling efficiency into mode k.

In order to describe the transverse field of a high M^2 laser beam we employ the Laguerre-Gaussian formulation which describes a free space laser mode as:

$$\mathbf{E}^{(\text{LG})}_l(\rho,\phi) = \vec{\mathbf{t}}\cdot\left(\frac{\rho\sqrt{2}}{w_0}\right)^{|m_l|}\exp\left(-\frac{\rho^2}{w_0^2}\right)L^{|m_l|}_{n_l}\left(\frac{2\rho^2}{w_0^2}\right)\exp(-im_l\phi) \tag{4}$$

where $\vec{\mathbf{t}}$ is the electric field polarisation vector, w_0 is the beam waist, m_l and n_l are the radial and azimuthal mode indices respectively of the l^{th} Laguerre-Gaussian mode and $L^m_n(x)$ is the Laguerre polynomial. As with the modes of an ARF the Laguerre-Gaussian modes form a complete, orthogonal set and, given the normalization of Eq. (1), we can describe the emitted laser beam, as a linear sum of those modes.

$$\mathbf{E}^{(\text{i})} = \sum_l c_l\mathbf{E}^{(\text{LG})}_l, \qquad \mathbf{H}^{(\text{i})} = \sum_l c_l\mathbf{H}^{(\text{LG})}_l \tag{5}$$

This description has the advantage that the M^2 value of a laser beam is obtained from its modal decomposition as [42]:

$$M^2 = \sum_l (1 + m_l + 2n_l)|c_l|^2 \tag{6}$$

For Eq. (6) to hold the beam must be propagating unit power, ie $\sum_l |c_l|^2 = 1$.

In Fig. 1 we show the number of mode groups required to be guided in a fiber to achieve our target of 95% coupling efficiency for a given incident beam, characterised by its M^2 value. A

Optics EXPRESS

beam with $M^2 = 15$ requires almost 100 mode groups. For this calculation the modes of the fiber are taken to be those of a hollow, circular fiber (a circular air hole in bulk silica, see the $N = 0$ structure in Fig. 3) as determined by Marcatili and Schmeltzer [43]. We conducted numerical simulation of a range of ARF geometries including tubular, NANF and DNANF and, although the transverse mode profiles, $\mathbf{E}_k$ and $\mathbf{H}_k$ in Eq. (1), are different for the same mode order in each of these structures, they all exhibited nearly identical requirements on the number of mode groups as that of the hollow circular fiber shown in Fig. 1. We find that a $M^2 = 3$ beam would require approximately 10 mode groups but the number of mode groups required to achieve the 95% coupling efficiency increases rapidly with M^2; an $M^2 = 10$ beam requires around 60 mode groups and M^2>15 requires more than 100 groups. In the next section we discuss how these requirements relate to ARF design.

It is clear from Eq. (6) that different combinations of the same modes, i.e. beams with different transverse fields, can result in equal M^2. Indeed, M^2 alone does not capture the richness of the corresponding mode field distributions. Figures 2(a)-(c) show three different possible modal distributions of an $M^2 = 3$ laser beam and the distribution in the modes of a fiber after coupling. The laser distributions are distinct and result in the excitation of different fiber modes. In Distributions 1 and 3 there is negligible power outside of the first 5 mode groups of the laser but for both distributions, more than 10% of the power is captured by mode group 6 and above in the fiber. Distribution 2 has the most evenly distributed power initially and is the most similar to the final distribution in the fiber. We show in Fig. 2(d) how the different laser beam distributions affect the coupling efficiency into the fiber as a function of the beam waist ratio, defined as the ratio between the laser beam waist and the fiber core radius, w_0/R. Regardless of the exact modal distribution, the same number of fiber modes is capable of capturing >95% of the beam. The maximum difference between the distributions shown here is 5% but at the optimum beam waist ratio the discrepancy is less than 1% and generally the results are nearly identical across the entire range. Note that beams with increased higher-order mode content are optimally coupled at smaller values of beam waist to core radius ratio, w_0/R. Coupling to single-mode beams is known to be maximised near $w_0/R = 0.7$ [44] whereas this $M^2 = 3$ beam has a maximum coupling at $w_0/R = 0.45$.

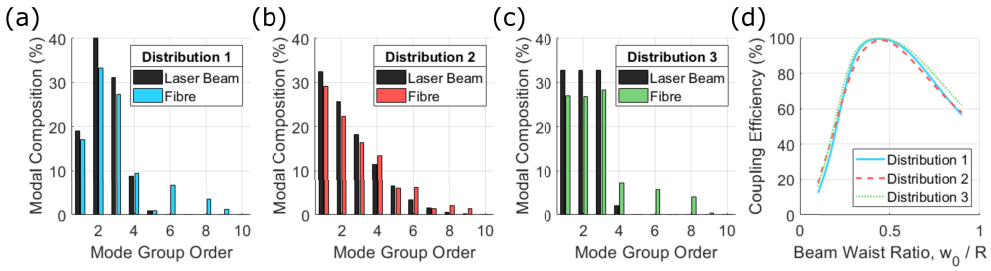

Fig. 2. (a)-(c) Several different modal distributions of (black bars) laser beams with $M^2 = 3$ before and (colored bars) after coupling into a fiber. (a) Distribution 1 and (b) Distribution 2 are described by discrete Gaussian functions with standard deviation 1 and 3 respectively and mean chosen to achieve the target M^2. (c) Distribution 3 is flat across lower order modes with the power of the highest order mode chosen to achieve the target M^2. (d) The total coupling efficiency of the beams described by (a)-(c) incident on a 10 mode fiber as a function of the beam waist ratio.

Throughout the research for this work, we investigated a range of input beams and found that for all metrics we explored, M^2 is a robust measurement with beams of diverse modal composition but equal M^2 achieving similar coupling efficiency into the fibers. Given the similarity between

Optics EXPRESS

results, we henceforth use for the remainder of the paper the modal decomposition described by the parameters of Distribution 2.

3. Multi-mode ARF design for high power laser delivery

In this section we present a design process for NANFs to guide the number of modes required to effectively capture and guide radiation from a multi-mode, high power laser. We derive a minimum core size requirement and describe how to design the cladding of a NANF to achieve multi-mode guidance.

3.1. Minimum core size

To determine the core size of the fiber, we first start by defining the maximum acceptable loss coefficient suitable for the intended application. Throughout this work we only consider losses due to confinement or leakage. Because of the larger cores, surface scattering remains negligible [4] and whilst microbending increases rapidly with core size [45], we speculate that these fibers could be packaged in such a way its contribution is also negligible. For MM guidance we must design the fiber such that all modes have losses below this threshold. Since, generally, the highest order mode will have the highest loss [46] and knowing the highest order mode from the coupling requirements, Fig. 1, we need only design such that that mode is below the loss threshold.

The leakage loss of an ARF geometry which consists of concentric rings of air and glass has been determined in closed form by Bird [47]. Most ARFs of interest cannot be modelled analytically. However, by considering the most similar concentric ring structure, with equal number of anti-resonant layers, we can make an estimate of the loss of a mode in decibels per unit length from [47]:

$$\alpha = \frac{20}{\ln 10}\left(\frac{x_0}{2\pi}\right)^{N+2}\frac{\epsilon_r^{N+1}+1}{2(\epsilon_r-1)^{(N+1)/2}}\frac{\lambda^{N+2}}{R^{N+3}}\prod_{i=1}^{N}\frac{1}{\sin^2(\phi_i)} \tag{7}$$

with R the core radius, λ the wavelength and ϵ_r the relative dielectric constant of the glass regions. The variable x_0 is a number determined by the mode; for the HE_{mn} mode it is the n^{th} zero of the Bessel function J_{m-1}. The geometry is characterised by N which is the integer number of finite concentric rings (including both air and glass regions) which make up the cladding (see Fig. 3 for examples). For the hollow circular fiber considered in the previous section $N = 0$, whilst for tubular, NANF and DNANF structures N most closely resembles 3, 5 and 7 respectively [4,36] (note that N is independent of the number of sets of nested capillaries surrounding the core). The final product term in Eq. (7) extends over the cladding regions and in this work we take $\phi_{\text{glass}} = 2\pi t\sqrt{\epsilon_r - 1}/\lambda$ and $\phi_{\text{air}} = \pi/2$. The thickness of the thin glass capillaries, t, controls the location of the high-loss resonant wavelengths, between which there are low-loss anti-resonant windows of operation [48]. To target an operating wavelength of 1030 nm, we choose a membrane thickness $t = 350$ nm that corresponds to a normalised frequency, $F = 0.71$ ($F = 2t/\lambda\sqrt{\epsilon_r - 1}$) placing 1030 nm near the expected minimum loss of the fundamental anti-resonant window [48]. The choice of ϕ_{air} corresponds to an "optimal" width of the air regions in the concentric ring structure (see [47]). Whilst there is no simple equivalent concept of an optimal width of air regions in NANF, they have been demonstrated to have lower losses for the same core size than even the most optimal concentric ring structure [4].

Figure 3 shows for a range of geometries the minimum core diameter, determined by Eq. (7), to guide 10, 30, 60 and 100 mode groups below a threshold of 10 dB/km. The 10 dB/km threshold is chosen such that these fibers will be capable of delivering power over 100 m with lower than 1 dB propagation losses. In reality we expect practical fibers to have lower confinement loss since tubular, NANF and DNANF structures generally have reduced leakage compared to the most similar concentric ring structures. Equation 7 suggests that tubular fibers with core diameters

Optics EXPRESS

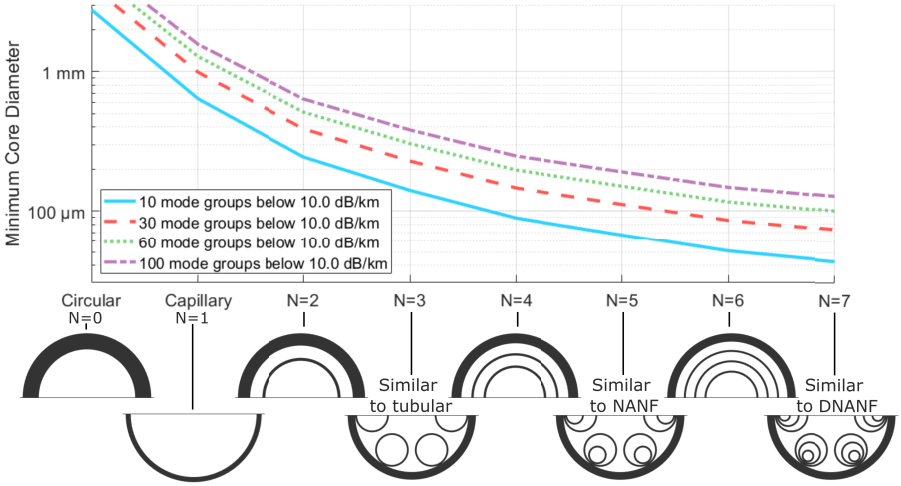

Fig. 3. The predicted minimum core size, according to Eq. (7), in order to guide 10, 30, 60, or 100 mode groups with a maximum loss less than 10 dB/km at 1030 nm for different ARF structures.

of 140 µm can support up to 10 mode groups and hence could be made to efficiently capture light from $M^2 \leq 3$ sources. As with solid-core fibers however, the additional loss due to bending increases with the size of the core in ARFs [49]. Such large core tubular fibers suffer from very severe bend loss.

A NANF with a core diameter of 150 µm is predicted to guide at least 60 mode groups, whilst 10 mode groups can be guided with a core diameter of around 70 µm. In addition to the smaller core size, NANFs are well known to have significantly improved bending resilience compared to tubular fiber (eg more than 4 orders of magnitude lower losses for 80 µm core diameter at 8 cm bend radius [4,49]). Figure 3 shows that to guide 100+ mode groups a NANF would require a core diameter of approximately 300 µm. Such large core NANFs have higher bend loss and are not capable of low-loss, multi-mode operation with a 35 cm bend radius. If we desire to guide a few 100 mode groups in an ARF, Eq. (7) suggests that DNANF might be the structure of choice, with smaller core requirements and even better resilience to bending compared to the NANF [3]. We leave for future work the task of investigating this solution that may be capable of guiding similar number of modes to MM solid-core fiber and be suitable for delivering laser light from highly multi-mode, $M^2>15$ sources. In this work we target laser sources with $M^2<15$ and therefore limit ourselves to studying NANFs with fewer than 100 mode groups.

There are other possible geometries that might be considered when designing MM ARF, such as the recently proposed centro-symmetric nested element structure [50]. NANFs, however, are a proven technology with 100s of km of single-mode fiber produced in the lab and commercial NANF cables already available. In this work we will focus on this design, due to the simplicity of its structure with a few, well understood parameters. In the next section we propose an effective technique for designing the cladding of multi-mode NANFs.

3.2. Cladding design

When designing NANFs it is necessary to correctly size the cladding features, each of which guide its own set of air modes. Single-mode NANFs are designed such that higher-order core modes are strongly coupled to the high loss cladding modes guided inside and in the gaps between tubes, so that the undesired high-order core modes are effectively stripped from the fiber [4]. To make a MM NANF coupling to cladding modes must instead be avoided, which can be achieved

Optics EXPRESS

by increasing the difference in effective index between the highest order core mode and the fundamental mode of the tube assembly in the cladding [46].

The two most significant air regions in the cladding of a NANF are between large and small capillaries and inside the small ones. When these regions are larger the effective index of the cladding modes guided within is greater and the difference in effective index between these modes and the core modes is decreased. Therefore we calculate the maximum size of cladding tube in order to maintain adequate effective index separation. We have found that a difference of 2×10^{-4} between the core and cladding modes is easily sufficient to avoid coupling [46]. We approximate the effective index of the core and cladding modes using [51]:

$$\mathrm{Re}(n_{\mathrm{eff}}^{(q)}) = n_{\mathrm{air}} - \frac{x_0^2}{2}\left[\frac{1}{n_{\mathrm{air}}}\left(\frac{\lambda}{2\pi R_q}\right)^2 + \frac{1}{n_{\mathrm{air}}^2}\left(\frac{\lambda}{2\pi R_q}\right)^3 \frac{\epsilon_r+1}{\sqrt{\epsilon_r-1}}\cot(\phi_{\mathrm{glass}})\right],\ q = \mathrm{core, cladding} \tag{8}$$

Numerical simulations indicate that the effective index of the significant cladding modes are approximately equal when $Z_1/Z_2 = 0.7$ (see definitions in Fig. 4(a)) and under this assumption we need only consider the small, nested capillary. Therefore for the cladding $R_{\mathrm{cladding}} = Z_2$ and $x_0 = 2.405$ (the first zero of the Bessel function $J_0(x)$) whilst for the core mode $R_{\mathrm{core}} = R$ and x_0 is that of the highest order mode desired to be guided (see x_0 definition in Eq. (7)). We also employ a refractive index model to account for the bending induced modification of the cladding mode refractive index by setting $n_{\mathrm{air}} = 1 + (R_{\mathrm{core}} + Z_1 + 2t + 0.5Z_2)/R_{\mathrm{bend}}$ when calculating the cladding mode effective index [49].

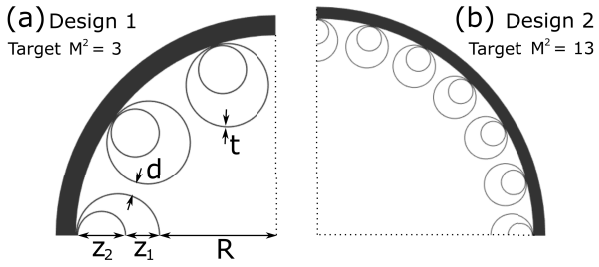

Fig. 4. Geometry of (a) design 1, a 10 mode group fiber and (b) design 2, a 62 mode group fiber.

4. Performance of multi-mode NANF for laser delivery

To assess the performance of MM NANFs for laser delivery and demonstrate our design techniques we design two fibers at the extremes of the M^2 range of interest. Figure 4 shows the cross section of Design 1 and Design 2, chosen using the techniques of Section 3. to deliver power from a laser with $M^2 = 3$ and $M^2 = 13$, respectively. To efficiently guide light from lasers with such parameters the fibers are required to guide 10 and 62 mode groups, respectively (see Fig. 1). Using Eq. (8) to avoid coupling to cladding modes we set Z_2 to 7 µm and 6 µm, respectively and $Z_1/Z_2 = 0.7$. We choose a gap size, $d = 4$ µm, comparable to recently fabricated NANFs [1]. With there parameters we find that the minimum core diameter requirement can be met with 10 and 24 tubes for Design 1 and 2, resulting in core diameters of 69 and 176 µm, respectively.

To check if fibers designed with the proposed method exhibit the desired properties, we performed numerical simulations of Design 1 and 2 using the commercial finite-element solver COMSOL Multiphysics. Here bend loss is calculated directly by imposing a conformal transformation to the refractive index [52].

Optics EXPRESS

4.1. Propagation and bending loss

Figure 5(a) shows the loss spectrum of the highest loss modes of the fibers when straight. Minimum leakage loss is 1.4 dB/km at 1050 nm for Design 1 and 0.8 dB/km at 1030 nm for Design 2. Loss increases at shorter wavelengths as the edge of fundamental anti-resonant window is approached. At 970 nm, the increase in loss is less than 0.3 dB/km for both designs. The available bandwidth is suitable not only for CW lasers, but also for ultrashort pulsed ones operating between 1030 and 1064 nm (a 100 fs Gaussian pulse at 1064 nm has a bandwidth of less than 20 nm). Figure 5(b) shows the maximum loss across all modes of the fibers for a range of bend radii. The critical bend radius, at which the loss is doubled compared to the straight fiber, for Design 2 is 35 cm and for Design 1 is less than 25 cm. The similarity between Design 1 and 2 in the dependence of loss with bend radius suggests that the additional loss experienced when bending the fiber is primarily due to phase matching to cladding modes. When the fiber is bent to a smaller radius, the real component of the effective index of the cladding modes in the tubes on the outside of the bend increases, Eq. (8), whereas the effective index of the core modes is approximately unchanged (smaller bends than those considered here may also modify the effective index of the core modes) [49]. Consequently the core and cladding modes have increased phase matching and the loss of the core modes increases [46]. Both designs demonstrate strong resilience to bending and are below the design threshold of 10 dB/km for bend radii as small as 25 cm radius. This is below the expected minimum bend radius in practical situations where the fiber is deployed in a protective cable and we do not expect bend loss to be a limitation.

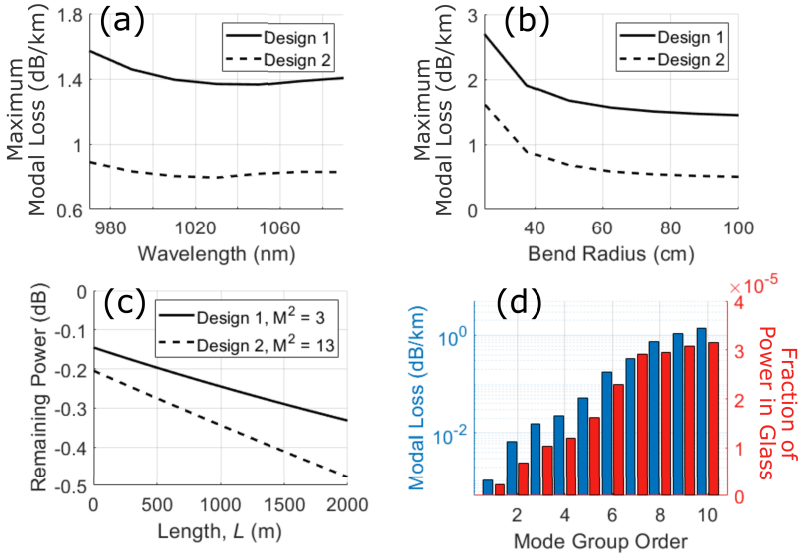

Fig. 5. (a) The maximum modal loss across all modes of Design 1 and 2 when straight. (b) The maximum modal bending loss at 1030 nm across all modes of Designs 1 and 2. (c) Delivered power after coupling and propagation for a $M^2 = 3$ beam incident on Design 1 and a $M^2 = 13$ beam incident on Design 2. Loss values consider a constant 35 cm bend. (d) The maximum leakage loss (blue bar, left axis) and the fraction of power in the glass (red bar, right axis) of all mode groups of Design 1 at 1030 nm when straight.

To better capture the throughput capability of the fiber when used in laser delivery, we have plotted in Fig. 5(c) the delivered output power after coupling and propagation for a $M^2 = 3$ beam incident on Design 1 and a $M^2 = 13$ beam incident on Design 2. The loss values shown here are calculated for a fiber coiled at a constant 35 cm radius bend. In both cases the initial power

Optics EXPRESS

loss value at the propagation distance $L = 0$ is due to input coupling and will be discussed later. In these calculations we have not included the effects of power coupling between the modes of the fiber. Under these assumptions, in both designs, after 2 km of propagation the total loss is predicted to be less than 0.5 dB and the leakage loss is less than 0.14 dB/km. Given such low leakage loss it is reasonable to assume that microbending, which increases rapidly with core size [45], will become the dominant source of propagation loss. Although the impact of microbending can be reduced or mitigated with choice of fiber packaging, given the lack of relevant experimental or theoretical data on large core, multi-mode ARF, we restrict ourselves in this work to studying the effects of differential leakage loss and multi-mode guidance. We note that the effective leakage loss is almost an order of magnitude less than the loss of the highest order mode. We can understand this result by considering Fig. 5(d) that shows the confinement losses of the 10 mode groups of Design 1 at 1030 nm. The loss of lower order modes is significantly less than the highest order mode, indeed the loss of the fundamental mode of Design 1 is nearly 3 orders of magnitude lower than the highest order mode. When launching power into MM fiber the low order fiber modes capture a significant fraction of the laser power (see Fig. 3) and so the total loss is consequently lower than that of the highest order mode. The fraction of power that propagates in the glass is shown in the right axis of Fig. 5(d) and increases with mode order. The glass fraction for the highest order modes is less than 4×10^{-5}, similar to the fundamental mode in single-mode NANFs [4], and the nonlinear contribution from silica is not expected to increase in multi-mode ARFs. Increased glass overlap has an effect on dispersion which is discussed in Section 4.4.

We also considered the M^2 of the laser beam at the output of the fiber and found that there was a negligible change compared to the incident beam, due to the extremely low, < 0.5 dB, losses. The effects of power coupling between the modes of the fiber may modify the output M^2 [37]. Most applications using these large M^2 sources will be tolerant to small changes in beam quality as measured by M^2. If necessary, the guidance mechanism of ARF does suggest a means of limiting the maximum output M^2 by designing the fiber such that any undesired modes, those with higher order than the initial design, have high enough losses that any power in those modes will be lost after propagation through the length of the fiber. The output M^2 would therefore be effectively limited by the highest order, low-loss fiber mode. This technique could be used to counter the effects of intermodal coupling or indeed to spatially filter the laser source, improving its M^2. Although this would incur additional power loss, it might be more desirable to develop longitudinal cooling techniques to dissipate power over the length of the fiber rather than at the fiber coupling where it can result in dangerous heat build-up. We leave for future work the task of investigating this possibility.

4.2. Coupling efficiency

In an industrial environment the coupling between the laser and fiber will generally experience variations in focus and alignment due to eg. thermal fluctuations and mechanical vibration. Maintaining coupling in these conditions is important if the fiber is to avoid thermal buildup due to lost power at the coupling and maintain the throughput power delivered to the workstation. We now consider the behaviour of the fiber when the incident beam is perturbed from optimal focus and alignment. The coupling efficiency of Design 1 for a $M^2 = 3$ beam at different values of beam waist ratio, w_0/R, is shown in Fig. 6(a). The coupling efficiency decreases as beam waist departs from the optimum, $w_0/R = 0.48$, where it reaches 96%. For Design 1, a change in beam waist of ±7% still results in 95% coupling or above. We show in Fig. 6(c) the coupling efficiency for Design 1 as an incident $M^2 = 3$, $w_0/R = 0.48$ beam is offset transversely. The coupling efficiency at zero offset, 96% (the optimum described above), decreases as alignment offset increases. We observe moderate tolerance to misalignment: a beam with a transverse offset of 10% of the core radius still achieves 95% coupling efficiency. The offset beam excites the fiber

Optics EXPRESS

modes differently, with more power coupled into the higher order modes which increases the effective loss of the fiber. Input coupling remains the dominant source of loss, however, and the total loss over 2 km with 10% transverse offset is less than 0.2 dB greater than an ideal launch with no offset.

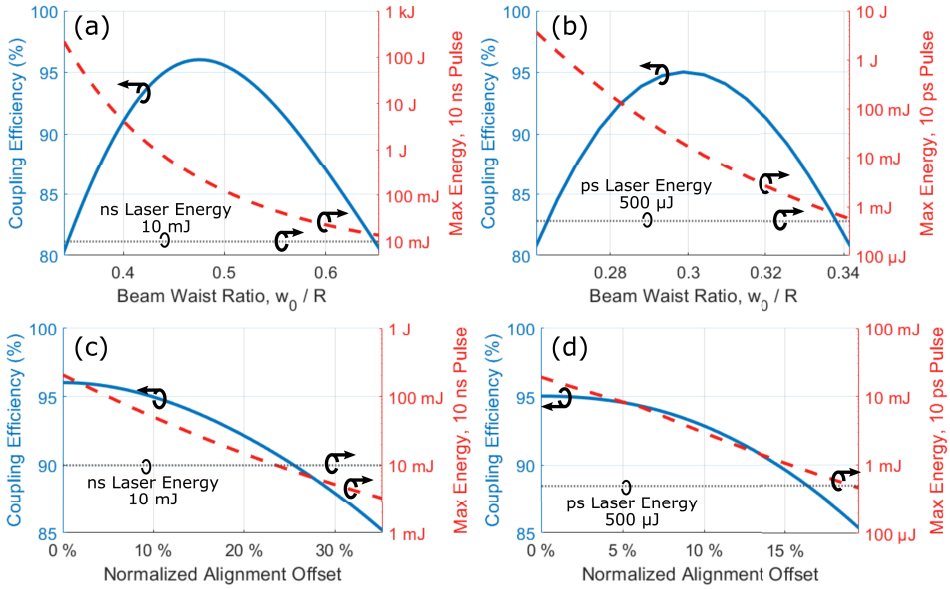

Fig. 6. The coupling efficiency (blue solid) and maximum pulse energy (red dashed) before damage for (a),(c) a 10 ns, $M^2 = 3$ pulse incident on Design 1 and (b),(d) a 10 ps, $M^2 = 13$ pulse incident on Design 2. The beam is modified by varying (a),(b) the beam waist ratio at zero alignment offset or (c),(d) the alignment offset at optimal beam waist. Alignment offset is normalized relative to the fiber core radius. The horizontal dotted line indicates the maximum pulse energies of high-energy, commercial nanosecond and picosecond lasers. [39,53].

In Fig. 6(b) and Fig. 6(d) we show for Design 2 and a $M^2 = 13$ beam the behaviour of coupling efficiency with variation in focus and misalignment respectively. The results are qualitatively similar to that of Design 1; there is an optimal beam waist and the coupling efficiency decreases with detuning from optimum focus or increasing transverse offset. The maximum coupling efficiency is 95%. When the transverse misalignment is 10% of the core radius or the focus is ±5% from optimal, coupling efficiency is 2.5% lower than maximum. The increased higher order mode content of the $M^2 = 13$ beam results in a smaller optimal beam waist ratio, $w_0/R = 0.30$ compared to the $M^2 = 3$ beam used with Design 1. The maximum coupling efficiency and tolerance to misalignment and focus is improved by guiding more modes in the fiber.

4.3. Damage threshold for pulsed lasers

The light induced damage threshold (LIDT) of an ARF is the maximum power it can withstand before the intensity on the glass microstructure exceeds the LIDT of bulk silica. In this work we take the LIDT of bulk silica to be 100 J/cm2 at 1030 nm for a 8 ns pulse [54]. Experimental work on microstructured hollow-core fibers suggests that this is a conservative limit, with 3x higher values being reported [14].

The dashed red lines in Fig. 6 show the LIDT of Designs 1 and 2 as the focus and alignment is modified with nanosecond and picosecond pulses, respectively. The maximum 10 ns pulse energy for Design 1 at optimal coupling is 230 mJ, a peak power of more than 20 MW. Due to

Optics EXPRESS

the low glass overlap, the LIDT of the NANFs is well above the achievable power from CW lasers. Therefore, here we consider instead the case of pulsed lasers which produce significantly higher peak powers. The LIDT behaves significantly differently to what might be expected in solid-core fibers since the peak optical intensity in the core does not damage the microstructure. In Figs. 6(a),(b) the damage threshold increases dramatically as the laser is more tightly focused since the intensity is reduced at the core/cladding interface. For Design 1 the maximum 10 ns pulse energy at $w_0/R = 0.5$ is 100 mJ, at $w_0/R = 0.45$ it is 500 mJ and at $w_0/R = 0.4$ it is more than 4 J. We also found that there was little improvement from higher M^2 beams that have a more flat-top profile since by far the dominant effect was that of focus. This means that the practical damage threshold can be significantly increased in MM ARF compared to few-mode or single-mode fibers since with more modes, tighter laser focus is possible while maintaining high coupling efficiency. This is evident in Fig. 6(a) which shows that the maximum pulse energy for 10 ns pulses at optimal coupling is 230 mJ but by decreasing the laser focus by just 7%, the coupling is still above 95% but the maximum pulse energy before damage increases to 650 mJ. For comparison, we chose a very high-energy nanosecond laser emitting at 1060 nm wavelength with a reported beam M^2 suitable for coupling to this fiber. The commercially available IPG Photonics YLPN has a maximum pulse energy of 10 mJ with a duration of 30 ns and requires a solid-core delivery fiber with a core diameter of 400 μm (more than 5x larger than that of Design 1) [39]. We note that even at optimal coupling the maximum pulse energy is already more than an order of magnitude higher than the YLPN and other typical nanosecond pulse lasers [7].

Figure 6(b) shows the LIDT of Design 2 when delivering 10 ps pulses. We find that the maximum pulse energy before damage of Design 2 at optimal coupling is almost 20 mJ. The high energy, commercially available, Trumpf TruMicro 2070 picosecond laser has a maximum pulse energy of 500 μJ [53]. We believe that suitably designed MM ARF fibers would be capable of handling the typical powers used in most applications and laser sources currently available, with considerable margins for further laser power up-scale.

Finally, as one might expect, Figs. 6(c),(d) show that the damage threshold decreases as alignment offset increases; for Design 1 a misalignment of 15% of the core radius results in almost an order of magnitude decrease in damage threshold. If large misalignment tolerances are required it may be therefore necessary to tighten the laser focus to maintain the damage thresholds.

4.4. Impact of dispersion on short pulse delivery

The delivery of nanosecond and picosecond pulses requires that we consider the dispersive properties of the fiber, as these may induce significant pulse broadening, thus lowering the output peak power and distorting the temporal profile of the pulses. Although single mode ARFs generally have lower dispersion compared to their solid-core counterparts, the dispersion increases markedly for higher-order modes. Furthermore, when operating in a few-mode or multi-mode regime, we must also consider the effect of intermodal differential group delay (DGD). Both dispersion and DGD increase approximately linearly with mode order [43]. Figure 7 shows the chromatic dispersion and DGD of the highest order modes of Designs 1 and 2. Design 2 guides more modes than Design 1, and this would increase both its maximum DGD and dispersion. This is however offset by the larger core which commensurately decreases both values [43]. It follows therefore that both designs offer similar values of maximum DGD and dispersion for the high order mode with the highest loss.

We consider the two cases described in Section 4.2: 10 ns pulses propagating in Design 1 and 10 ps pulses propagating in Design 2. When calculating dispersion, we assume that all power is propagating in the highest order mode which constitutes the worst possible case. The dispersion experienced by a short pulse will depend on the precise coupling conditions and, if present,

Optics EXPRESS

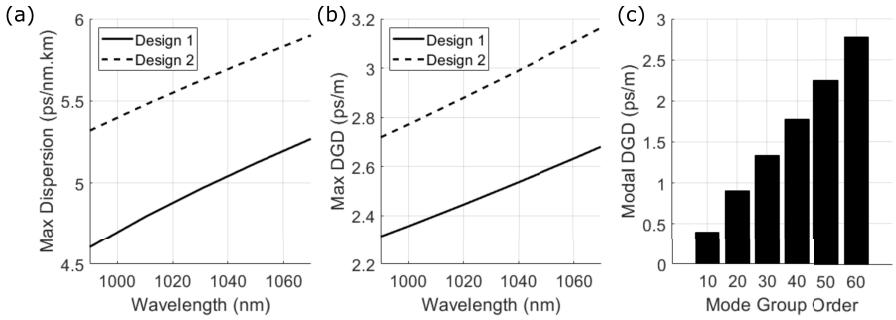

Fig. 7. For the highest order modes of Design 1 and 2 (a) the dispersion parameter, D, and (b) the differential group delay as a function of wavelength. (c) the DGD of every tenth mode group in Design 2 at 1030 nm.

intermodal power coupling along the length of the fiber. However, the case of uncoupled modes with the greatest DGD which we consider here represents again a worst-case scenario.

The dispersion length, $L_D = \frac{2\pi c_0}{\lambda^2}\frac{\tau_0^2}{|D|}$, for an initially unchirped, temporally-Gaussian pulse of duration τ_0 propagating in a waveguide with dispersion D, is defined as the distance over which the duration of that pulse increases by a factor of $\sqrt{2}$. For a 10 ps pulse in Design 2 the dispersion length is over 3 km for the highest order mode whilst for a 10 ns pulse the value is 6 orders of magnitude larger. Clearly chromatic dispersion will not have a significant impact on propagation.

Considering DGD, we can define the dispersion length, $L_{DGD} = \frac{\tau_0(\sqrt{2}-1)}{|DGD|}$ for a square wave of duration τ_0 with 50% of power in the fundamental fiber mode and 50% power in the highest order mode as the distance over which the duration of that pulse increases by a factor $\sqrt{2}$. For Design 1 a 10 ns pulse has $L_{DGD} = 1.7$ km. A 10 ps pulse propagating in Design 2 has $L_{DGD} = 1.4$ m. Although this is a worst-case scenario estimation, the DGD will clearly be the limiting factor for delivering high-power, low beam quality pulses of picosecond duration in MM ARFs. The DGD can be reduced in ARF by increasing the size of the core or by reducing the number of modes in which power is guided. In Fig. 7(c) we show the DGD in Design 2 of every tenth mode group relative to the fundamental mode (other groups are omitted for clarity of reading). The dependence on mode order is approximately linear. Picosecond duration pulsed lasers generally have lower M^2 values than what we have so far assumed; if we consider a 10 ps pulse with $M^2 = 3$, very similar to [26], then more than 95% of the power is coupled into the first 10 mode groups. Taking the DGD as that of the tenth mode group then $L_{DGD} = 10.5$ m, comparable to the maximum lengths of typical solid-core power-delivery fiber. Despite the high DGD compared to solid-core fibers, MM ARF permits order of magnitude higher damage thresholds and more flexible fibers due to the low bending loss, < 2.5 dB/km at 35 cm bend radius, and smaller core size, eg Design 1 has a 5x smaller core than comparable fibers for nanosecond delivery [39].

5. Conclusions

We have presented a technique for the design of MM ARFs for high-power fiber-delivery of few- and multi-moded laser sources. Using this technique we designed, as an example, two MM NANFs for use with beams of $M^2 = 3$ and 13. We have assessed the performance of these fibers using numerical simulation and found them both to satisfy the design requirement, confirming the validity of the design method. Both fibers can provide > 95% coupling efficiency to their multi-mode laser inputs. Besides, both can deliver power with negligible leakage loss whilst tolerating bends with radii under 35 cm and seem capable of multi-km flexible laser delivery with little loss. Delivery of 10s of kW power over multi-km distances presents several opportunities in

Optics EXPRESS

novel and existing applications. For example in situations, such as nuclear decommissioning, where the laser processing target is difficult or hazardous to access [55] or for subsurface rock drilling for the extraction of gas and oil [56]. Equally, in existing factory machining applications, such long distance delivery offers greater flexibility; high-power lasers, and their associated power and cooling requirements, could be physically removed from the production line. In applications demanding shorter distances, the size of the core can be reduced without sacrificing coupling efficiency. For example if Design 1 were modified to have a 60 µm core diameter it would still be capable of delivering an $M^2 = 3$ beam with < 0.5 dB loss over at least 100 m whilst also increasing the flexibility of the fiber.

The damage threshold of the fibers considered here are between 20x and 40x greater than current typical requirements of nanosecond and picosecond pulses and can be increased significantly further if the fibers are designed to guide more modes. The DGD of the highest order modes is likely to limit the reach of picosecond pulses to 10 m but we believe this can be mitigated by increasing the core size, although this may reduce the degree of bending the fiber can tolerate.

This work demonstrates that MM ARFs are capable of delivering radiation from high-power laser sources with large M^2 beams over significantly larger distances and with greater power damage thresholds than current solid-core fibers and do so with similar or improved flexibility.

Funding. Royal Academy of Engineering; Engineering and Physical Sciences Research Council.

Acknowledgments. ENF acknowledges support from a Royal Academy of Engineering University Research Fellowship. FP gratefully acknowledges funding from the ERC project Lightpipe (grant number 682724).

Disclosures. The authors declare no conflicts of interest.

Data availability. Data underlying the results presented in this paper are available in Ref. [57].

References

1. G. T. Jasion, T. D. Bradley, K. Harrington, H. Sakr, Y. Chen, E. N. Fokoua, I. A. Davidson, A. Taranta, J. R. Hayes, D. J. Richardson, and F. Poletti, "Hollow Core NANF with 0.28 dB/km Attenuation in the C and L Bands," in *Optical Fiber Communication Conference Postdeadline Papers 2020*, (Optical Society of America, 2020), paper Th4B.4.
2. H. Sakr, T. D. Bradley, G. T. Jasion, E. N. Fokoua, S. R. Sandoghchi, I. A. Davidson, A. Taranta, G. Guerra, W. Shere, Y. Chen, J. R. Hayes, D. J. Richardson, and F. Poletti, "Hollow Core NANFs with Five Nested Tubes and Record Low Loss at 850, 1060, 1300 and 1625nm," in *Optical Fiber Communications Conference and Exhibition (OFC)* (2021), pp. 1–3.
3. G. T. Jasion, H. Sakr, J. R. Hayes, S. R. Sandoghchi, L. Hooper, E. N. Fokoua, A. Saljoghei, H. C. Mulvad, M. Alonso, A. Taranta, T. D. Bradley, I. A. Davidson, Y. Chen, D. J. Richardson, and F. Poletti, "0.174 dB/km Hollow Core Double Nested Antiresonant Nodeless Fiber (DNANF)," in *Optical Fiber Communications Conference and Exhibition (OFC)* (2022), pp. 1–3.
4. F. Poletti, "Nested antiresonant nodeless hollow core fiber," Opt. Express **22**(20), 23807 (2014).
5. A. Taranta, E. Numkam Fokoua, S. Abokhamis Mousavi, J. R. Hayes, T. D. Bradley, G. T. Jasion, and F. Poletti, "Exceptional polarization purity in antiresonant hollow-core optical fibres," Nat. Photonics **14**(8), 504–510 (2020).
6. V. Michaud-Belleau, E. Numkam Fokoua, T. D. Bradley, J. R. Hayes, Y. Chen, F. Poletti, D. J. Richardson, J. Genest, and R. Slavík, "Backscattering in antiresonant hollow-core fibers: over 40 dB lower than in standard optical fibers," Optica **8**(2), 216–219 (2021).
7. D. J. Richardson, J. Nilsson, and W. A. Clarkson, "High power fiber lasers: current status and future perspectives [Invited]," J. Opt. Soc. Am. B **27**(11), B63–B92 (2010).
8. J. W. Dawson, M. J. Messerly, R. J. Beach, M. Y. Shverdin, E. A. Stappaerts, A. K. Sridharan, P. H. Pax, J. E. Heebner, C. W. Siders, and C. P. J. Barty, "Analysis of the scalability of diffraction-limited fiber lasers and amplifiers to high average power," Opt. Express **16**(17), 13240–13266 (2008).
9. C. Rohrer, C. A. Codemard, G. Kleem, T. Graf, and M. A. Ahmed, "Preserving Nearly Diffraction-Limited Beam Quality Over Several Hundred Meters of Transmission Through Highly Multimode Fibers," J. Lightwave Technol. **37**(17), 4260–4267 (2019).
10. T. Okuda, Y. Fujiya, S. Goya, and A. Inoue, "Beam transmission technology by photonic crystal fiber to realizes high-precision and high-efficiency laser processing technology," Mitsubishi Heavy Ind. Tech. Rev **57**, 1–5 (2020).
11. IPG Photonics YLS, https://www.ipgphotonics.com/en/products/lasers/high-power-cw-fiber-lasers/1-micron/yls-1-120-kw. Accessed 4 July 2022.
12. S. A. Mousavi, H. C. H. Mulvad, N. V. Wheeler, P. Horak, J. Hayes, Y. Chen, T. D. Bradley, S.-u. Alam, S. R. Sandoghchi, E. N. Fokoua, D. J. Richardson, and F. Poletti, "Nonlinear dynamic of picosecond pulse propagation in atmospheric air-filled hollow core fibers," Opt. Express **26**(7), 8866–8882 (2018).

Optics EXPRESS

13. L. F. Michaille, D. M. Taylor, C. R. H. Bennett, T. J. Shepherd, C. Jacobsen, and T. P. Hansen, "Damage threshold and bending properties of photonic crystal and photonic band-gap optical fibers," in *Proc. SPIE* vol. 5618 (2004).
14. P. Jaworski, F. Yu, R. R. J. Maier, W. J. Wadsworth, J. C. Knight, J. D. Shephard, and D. P. Hand, "Picosecond and nanosecond pulse delivery through a hollow-core Negative Curvature Fiber for micro-machining applications," Opt. Express **21**(19), 22742–22753 (2013).
15. M. Michieletto, J. K. Lyngsø, C. Jakobsen, J. Laegsgaard, O. Bang, and T. T. Alkeskjold, "Hollow-core fibers for high power pulse delivery," Opt. Express **24**(7), 7103–7119 (2016).
16. S. Eilzer and B. Wedel, "Hollow Core Optical Fibers for Industrial Ultra Short Pulse Laser Beam Delivery Applications," Fibers **6**(4), 80 (2018).
17. H. C. H. Mulvad, S. Abokhamis Mousavi, V. Zuba, L. Xu, H. Sakr, T. D. Bradley, J. R. Hayes, G. T. Jasion, E. Numkam Fokoua, A. Taranta, S.-U. Alam, D. J. Richardson, and F. Poletti, "Kilowatt-average-power single-mode laser light transmission over kilometre-scale hollow-core fibre," Nat. Photonics **16**(6), 448–453 (2022).
18. U. Brauch, C. Röcker, T. Graf, and M. Abdou Ahmed, "High-power, high-brightness solid-state laser architectures and their characteristics," Appl. Phys. B: Lasers Opt. **128**(3), 58 (2022).
19. V. Kuhn, T. Gottwald, C. Stolzenburg, S.-S. Schad, A. Killi, and T. Ryba, "Latest advances in high brightness disk lasers," Proc. SPIE **9342**, 93420Y (2015).
20. S. Nagel, B. Metzger, T. Gottwald, V. Kuhn, A. Killi, and S. S. Schad, "Thin disk laser operating in fundamental mode up to a power of 4kW," *Conference on Lasers and Electro-Optics Europe and European Quantum Electronics Conference* (2019).
21. A. Diebold, C. J. Saraceno, C. R. Phillips, F. Saltarelli, I. J. Graumann, and U. Keller, "Gas-lens effect in kW-class thin-disk lasers," Opt. Express **26**(10), 12648–12659 (2018).
22. R. Fleischhaker, R. Gebs, A. Budnicki, M. Wolf, J. Kleinbauer, and D. H. Sutter, "Compact gigawatt-class sub-picosecond Yb:YAG thin-disk regenerative chirped-pulse amplifier with high average power at up to 800 kHz," *Conference on Lasers and Electro-Optics Europe and International Quantum Electronics Conference* (2013).
23. D. Sutter, F. Krausz, M. Ueffing, R. Lange, T. Metzger, T. Nubbemeyer, T. Pleyer, V. Pervak, and Z. Major, "Direct regenerative amplification of femtosecond pulses to the multimillijoule level," Opt. Lett. **41**(16), 3840–3843 (2016).
24. O. H. Heckl, J. Kleinbauer, D. Bauer, S. Weiler, T. Metzger, and D. H. Sutter, "Ultrafast thin-disk lasers," Springer Series in Optical Sciences **195**, 93–115 (2016).
25. C. Herkommer, P. Krötz, R. Jung, S. Klingebiel, C. Wandt, R. Bessing, P. Walch, T. Produit, K. Michel, D. Bauer, R. Kienberger, and T. Metzger, "Ultrafast thin-disk multipass amplifier with 720 mJ operating at kilohertz repetition rate for applications in atmospheric research," Opt. Express **28**(20), 30164–30173 (2020).
26. A. Loescher, C. Röcker, M. A. Ahmed, and T. Graf, "Azimuthally polarized picosecond vector beam with 1.7 kW of average output power," Opt. Lett. **46**(14), 3492–3495 (2021).
27. T. Dietz, M. Jenne, D. Bauer, M. Scharun, D. Sutter, and A. Killi, "Ultrafast thin-disk multi-pass amplifier system providing 1.9 kW of average output power and pulse energies in the 10 mJ range at 1 ps of pulse duration for glass-cleaving applications," Opt. Express **28**(8), 11415–11423 (2020).
28. H. D. Hoffmann, J. Weitenberg, P. Russbueldt, R. Poprawe, and T. Mans, "Compact diode-pumped 1.1 kW Yb:YAG Innoslab femtosecond amplifier," Opt. Lett. **35**(24), 4169–4171 (2010).
29. P. Russbueldt, D. Hoffmann, M. Höfer, J. Löhring, J. Luttmann, A. Meissner, J. Weitenberg, M. Traub, T. Sartorius, D. Esser, R. Wester, P. Loosen, and R. Poprawe, "Innoslab Amplifiers," IEEE J. Sel. Top. Quantum Electron. **21**(1), 447–463 (2015).
30. B. E. Schmidt, A. Hage, T. Mans, F. Legare, and H. J. Worner, "Highly stable, 54mJ Yb-InnoSlab laser platform at 0.5kW average power," Opt. Express **25**(15), 17549–17555 (2017).
31. TRUMPF | TruDisk, https://www.trumpf.com/en_INT/products/laser/disk-lasers/trudisk/. Accessed 4 July 2022.
32. IPG Photonics YLS-SM, https://www.ipgphotonics.com/en/products/lasers/high-power-cw-fiber-lasers/1-micron/yls-sm-1-10-kw. Accessed 4 July 2022.
33. TRUMPF | TruPulse, https://www.trumpf.com/en_GB/products/laser/pulsed-lasers/trupulse/. Accessed 4 July 2022.
34. W. Shere, G. T. Jasion, E. N. Fokoua, and F. Poletti, "Low Loss, Large Bandwidth Antiresonant Hollow-Core Fiber Design for Short-Reach Links," *Optical Fiber Communication Conference (OFC)* (Optical Society of America, 2020), paper W4D.3.
35. P. Zhao, H. L. Ho, W. Jin, S. Fan, S. Gao, Y. Wang, and P. Wang, "Gas sensing with mode-phase-difference photothermal spectroscopy assisted by a long period grating in a dual-mode negative-curvature hollow-core optical fiber," Opt. Lett. **45**(20), 5660–5663 (2020).
36. B. Winter, T. A. Birks, and W. J. Wadsworth, "Multimode Hollow-Core Anti-Resonant Optical Fibres," in *Frontiers in Optics + Laser Science APS/DLS* (Optical Society of America, 2019), paper JTu4A.18.
37. M. A. Cooper, S. Wittek, D. Cruz-Delgado, J. Wahlen, J. M. Mercado, J. E. Antonio-Lopez, and R. A. Correa, "Higher order mode generation in an anti-resonant hollow-core fiber," in *Proc. SPIE* 11724 (2021).
38. Z. Dong, X. Zhang, P. Yao, J. Yao, S. Wan, and P. Wang, "Development of multi-mode rod-type hollow-core antiresonant fiber," in *Proc. SPIE* 12280 (2022).
39. IPG Photonics YLPN 1-10 mJ, 100-300 W, https://www.ipgphotonics.com/en/products/lasers/nanosecond-fiber-lasers/1-06-micron/ylpn-1-2-mj-100-300-w. Accessed 7 July 2022.
40. A. E. Siegman, "Defining, measuring, and optimizing laser beam quality," *Proc. SPIE* 1868 (1993).

Optics EXPRESS

41. V. Zuba, H. C. H. Mulvad, R. Slavík, H. Sakr, F. Poletti, D. J. Richardson, and E. N. Fokoua, "Experimental Investigation into Optimum Laser Coupling Efficiency into Hollow-Core NANFs," in *Conference on Lasers and Electro-Optics* (Optica Publishing Group, 2022), paper SW4K.1.
42. A. E. Siegman, "New developments in laser resonators," *Proc. SPIE* 1224 (1990).
43. E. A. J. Marcatili and R. A. Schmeltzer, "Hollow metallic and dielectric waveguides for long distance optical transmission and lasers," Bell Syst. Tech. J. **43**(4), 1783–1809 (1964).
44. E. N. Fokoua, R. Slavik, D. J. Richardson, and F. Poletti, "Limits of Coupling Efficiency into Hollow-Core Antiresonant Fibers," in *Conference on Lasers and Electro-Optics (CLEO)* (2021), pp. 1–2.
45. E. N. Fokoua, Y. Chen, D. J. Richardson, and F. Poletti, "Microbending effects in hollow-core photonic bandgap fibers," in *42nd European Conference on Optical Communication* (2016), pp. 1–3.
46. W. Shere, G. T. Jasion, E. Numkam Fokoua, and F. Poletti, "Understanding the impact of cladding modes in multi-mode hollow-core anti-resonant fibres," Opt. Fiber Technol. **71**, 102919 (2022).
47. D. Bird, "Attenuation of model hollow-core, anti-resonant fibres," Opt. Express **25**(19), 23215 (2017).
48. J. R. Hayes, F. Poletti, M. S. Abokhamis, N. V. Wheeler, N. K. Baddela, and D. J. Richardson, "Anti-resonant hexagram hollow core fibers," Opt. Express **23**(2), 1289 (2015).
49. M. H. Frosz, P. Roth, M. C. Günendi, and P. S. Russell, "Analytical formulation for the bend loss in single-ring hollow-core photonic crystal fibers," Photonics Res. **5**(2), 88–91 (2017).
50. C. Goel and S. Yoo, "Multimode nested antiresonant hollow core fiber," J. Lightwave Technol. **39**(20), 6592–6598 (2021).
51. M. Zeisberger and M. A. Schmidt, "Analytic model for the complex effective index of the leaky modes of tube-type anti-resonant hollow core fibers," Sci. Rep. **7**(1), 11761 (2017).
52. M. Heiblum and J. Harris, "Analysis of curved optical waveguides by conformal transformation," IEEE J. Quantum Electron. **11**(2), 75–83 (1975).
53. TRUMPF | TruMicro Series 2000, https://www.trumpf.com/en_GB/products/laser/short-and-ultrashort-pulse-lasers/trumicro-series-2000/. Accessed 7 July 2022.
54. F. Rainer, L. J. Atherton, J. H. Campbell, F. P. D. Marco, M. R. Kozlowski, A. J. Morgan, and M. C. Staggs, "Four-harmonic database of laser-damage testing," in *Proc. SPIE* 1624 (1992).
55. P. A. Hilton and A. Khan, "Underwater cutting using a 1 μm laser source," J. Laser Appl. **27**(3), 032013 (2015).
56. M. S. Zediker, "High power fiber lasers in geothermal, oil and gas," *Proc. SPIE* 8961 (2014).
57. W. Shere, G. T. Jasion, E. N. Fokoua, and F. Poletti, "Dataset for Designing multi-mode anti-resonant hollow-core fibers for industrial laser power delivery," University of Southampton (2022), https://doi.org/10.5258/SOTON/D2388.